J|A|C|S
ARTICLES
Published on Web 02/07/2003

Variety of the Molecular Conformation in Peptide Nanorings and Nanotubes

Hajime Okamoto,* Tsutomu Nakanishi, Yukiko Nagai, Maki Kasahara, and Kyozaburo Takeda*,†

Contribution from the Department of Materials Science and Engineering, School of Science and Engineering, Waseda University, Tokyo 169-8555, Japan

Received October 14, 2002; E-mail: okamoto@qms.cache.waseda.ac.jp, takeda@qms.cache.waseda.ac.jp

Abstract: Possible molecular conformations in peptide nanorings and nanotubes were theoretically investigated by a mathematical conformation analysis as well as ab initio Hartree−Fock calculations. The mathematical analysis predicts not only the conventional nanorings having an extended-type (E-type) backbone (trans zigzag) but also the novel ones having bound-type (B-type) backbones with a smaller internal diameter. Ab initio calculations for the amino acid substitution reveal that all 20 encoded residues can form both types of the above nanorings as a local minimum. However, the energetically stable type is determined in accordance with the kind of the replaced side chains. Moreover, the present work theoretically reveals that both types of nanorings stack to form nanotubes through inter-ring hydrogen bonds, i.e., larger E-type nanotubes and smaller B-type nanotubes. Electronically, the HOMO and LUMO states of the nanoring and nanotube backbones are formed by the in-plane π state. The replacement by the appropriate residues is furthermore predicted to intrude additional levels in the energy gap and to form the frontier states localized at the side chains.

I. Introduction

The progress of modern technology has been leading the physical components of machines and devices to dramatic miniaturization. Materials scientists are increasingly building nanoscale materials to discover new chemical and physical properties. In particular, nanotubular structures, such as carbon nanotubes, have been fueling much of this interest because of their potential utility in various areas. The design of nanotube structures has been desired not only in inorganic and/or organic fields but also in biomaterials. Peptide nanotubes (PNTs) are especially interesting artificial biomolecules having an open-ended hollow core. They are formed by the spontaneous stacking of peptide closed rings (PCRs), which consist of an alternate sequence of D- and L-amino acid residues (DL-peptide). Since the first synthesis in 1993 by Ghadiri et al.,[1] his group has been vigorously challenged to extend the new field of biomediated materials such as trans-membrane ion channels or drug delivery vehicles using the open-ended hollow core of the PNTs.[2−8]

On the contrary, we are focusing on their other new physical applications because of the flexibility in designing PCRs. Because the internal diameters and outside surface properties can be controlled by modifying the number and kind of constituent amino acid residues, the usage of the PNTs is open to other fields such as electronics. From this standpoint, we have discussed the electronic and molecular structures of the simplest homo-Gly PNT in our previous papers.[9,10] In that study, we understood the energetics as well as the electronic structures systematically from the viewpoint of the skeletal folding of the polypeptide chains, head-to-tail cyclization, and inter-ring interaction.

To determine the designing principle for new PNT structures, we here investigated the possible PCR backbones following the mathematical method of Shimanouchi and Mizushima[11] and also of Miyazawa.[12] Because this mathematical analysis provides the general relationship between the internal coordinate system and the external coordinate system in a polymer, one can find the possible steric conformation in terms of their internal parameters. Using this mathematical treatment, they have investigated the helical conformation for a homo sequence of L-amino acid residues. De Santis et al.[13] have also examined the steric conformation of an alternate sequence of D- and L-amino acid residues (DL-peptide) and have forecasted the existence of PCR and PNT forms mathematically. However, after their pioneering work, few studies have been performed to describe the detailed

† http://www.qms.cache.waseda.ac.jp. The structural data given by the present calculations are posted on the above web site.

(1) Ghadiri, M. R.; Granja, J. R.; Milligan, R. A.; McRee, D. E.; Khazanovich, N. *Nature* **1993**, *366*, 324.
(2) Ghadiri, M. R.; Granja, J. R.; Buehler, L. K. *Nature* **1994**, *369*, 301.
(3) Khazanovich, N.; Granja, J. R.; McRee, D. E.; Milligan, R. A.; Ghadiri, M. R. *J. Am. Chem. Soc.* **1994**, *116*, 6011.
(4) Ghadiri, M. R. *Adv. Matter.* **1995**, *7*, 675.
(5) Hartgerink, J. D.; Granja, J. R.; Milligan, R. A.; Ghadiri, M. R. *J. Am. Chem. Soc.* **1996**, *118*, 43.
(6) Clark, T. D.; Buehler, L. K.; Ghadiri, M. R. *J. Am. Chem. Soc.* **1998**, *120*, 651.
(7) Bong, D. T.; Clark, T. D.; Granja, J. R.; Ghadiri, M. R. *Angew. Chem., Int. Ed.* **2001**, *40*, 988.
(8) Fernandez-Lopez, S.; Kim, Hui-Sun; Choi, E. C.; Delgado, M.; Granja, J. R.; Khasanov, A.; Kraehenbuehl, K.; Long, G.; Weinberger, D. A.; Wilcoxen, K. M.; Ghadiri, M. R. *Nature* **2001**, *412*, 452.
(9) Fukasaku, K.; Takeda, K.; Shiraishi, K. *J. Phys. Soc. Jpn.* **1997**, *66*, 3387; *ibid.* **1998**, *67*, 3751.
(10) Okamoto, H.; Takeda, K.; Shiraishi, K. *Phys. Rev. B* **2001**, *64*, 115 425.
(11) Shimanouchi, T.; Mizushima, S. *J. Chem. Phys.* **1955**, *23*, 707.
(12) Miyazawa, T. *J. Polym. Sci.* **1961**, *55*, 215.
(13) De Santis, P.; Morosetti, S.; Rizzo, R. *Macromolecules* **1974**, *7*, 52.

10.1021/ja0212720 CCC: $25.00

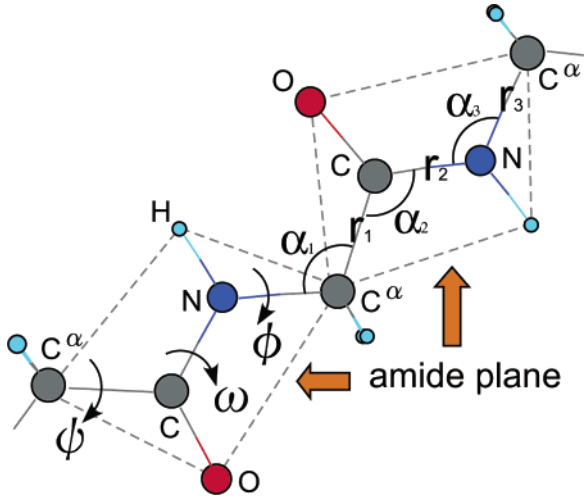

Figure 1. Illustration of the polypeptide chain. The internal parameters of the bond lengths r_i, the bond angles α_i ($i = 1, 2, 3$), and the internal rotation angles ϕ, ψ, and ω are shown in the figure. When $\omega = 180°$, a flat amide plane is produced between C^{α} atoms.

conformations for possible PCRs and PNTs. Furthermore, any discussion on the energetics including their stable molecular structures has not been provided yet.

In the present work, we investigated the possible backbone conformations of the DL-peptide attentively and examined new PCR and PNT structures by mathematical analysis as well as ab initio energy calculations. For this purpose, we first summarized the outline of our mathematical considerations on the backbone building. Next, we applied this treatment to the DL-peptide nanorings and discussed two possible backbones of the extended-type and the bound-type. We then carried out Hartree−Fock calculations and examined the energetically stable conformations of those PCR backbones. The effect of the amino acid substitution was, moreover, investigated for all 20 encoded residues, and the electronic structures of those homo-residue PCRs are discussed here. Finally, we carried out the geometry optimization of the PNTs and investigated the stable molecular conformations and their band structures.

II. Backbone Conformation of the Peptide Nanorings

First, we investigate the possible steric conformation of the periodic polypeptide in which D- and L-amino acid residues are catenated alternately (DL-peptide). This DL-peptide sequence basically causes *zero-transfer* helices (open rings), in contrast to the usual right-handed or left-handed helices in the homo-L-amino acid sequence. The *zero-transfer* helices have significant steric hindrance unless the DL-peptide sequence is closed per helical turn and does not place the individual atoms at the very same site. To close the N-terminus and C-terminus and form the PCR, an even number of amino acid residues is conventionally required for this periodic DL-peptide.[14] Thus, our first step is to obtain a generalized mathematical expression for this DL-peptide using helical pitch angle θ in terms of the internal parameters of the bond lengths r_i, the bond angles α_i ($i = 1, 2, 3$), and the internal rotation angles ϕ, ψ, and ω (Figure 1).

(14) Recentry, we mathematically predicted that the DL-peptide of $n = 5$ has a chance to close the backbone exceptionally.[15] However, the penta-DL-peptide does not have the S_n symmetry.

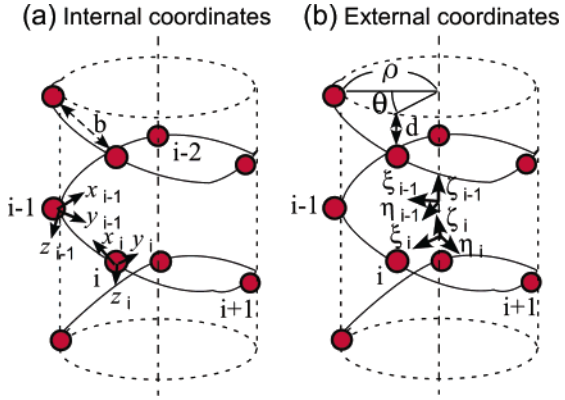

Figure 2. Illustration of a polymer backbone represented by internal orthogonal coordinate system (a) and by external orthogonal coordinate system (b).

A. Linear Transformation in Polypeptide. According to Shimanouchi and Mizushima[11] and also Miyazawa,[12] the coordinates of the backbone atoms are easily expressed in the form of a linear transformation, if the sequence of the backbone atoms has a periodicity. For the internal orthogonal coordinate system (Figure 2a), the coordinates of the $(i-1)$th atom (x_{i-1}, y_{i-1}, z_{i-1}) are expressed using the coordinates of the ith atom (x_i, y_i, z_i) as

$$\vec{X}_{i-1} = \boldsymbol{A}\vec{X}_i + \vec{B} \tag{1}$$

where $\vec{X}_i$ is a column vector with elements x_i, y_i, and z_i. **A** is an orthogonal matrix defined by

$$\boldsymbol{A} = \begin{pmatrix} a_{11} & a_{12} & a_{13} \\ a_{21} & a_{22} & a_{23} \\ a_{31} & a_{32} & a_{33} \end{pmatrix} \tag{2}$$

and $\vec{B}$ is a transfer vector given by

$$\vec{B} = \begin{pmatrix} b \\ 0 \\ 0 \end{pmatrix} \tag{3}$$

An analogous relation is also found in the external orthogonal coordinate system (Figure 2b). In this case, the transformation of $\vec{\xi}_i$ into $\vec{\xi}_{i-1}$ is expressed as

$$\vec{\xi}_{i-1} = \boldsymbol{N}\vec{\xi}_i + \vec{D} \tag{4}$$

where **N** is an orthogonal matrix determined by a helical pitch angle θ as

$$\boldsymbol{N} = \begin{pmatrix} \cos\theta & -\sin\theta & 0 \\ \sin\theta & \cos\theta & 0 \\ 0 & 0 & 1 \end{pmatrix} \tag{5}$$

and $\vec{D}$ is a transfer vector

$$\vec{D} = \begin{pmatrix} 0 \\ 0 \\ d \end{pmatrix} \tag{6}$$

Here, the transformation of $\vec{\xi}_i$ into $\vec{X}_i$ is calculated by

$$\vec{X}_i = \boldsymbol{T}(\vec{\xi}_i + \vec{S}) \tag{7}$$

where **T** is an orthogonal matrix whose elements are determined so as to make three eqs 1, 4, and 7 consistent

$$\boldsymbol{T} = \begin{pmatrix} t_{11} & t_{12} & t_{13} \\ t_{21} & t_{22} & t_{23} \\ t_{31} & t_{32} & t_{33} \end{pmatrix} \tag{8}$$

and $\vec{S}$ is a transfer vector given by

$$\vec{S} = \begin{pmatrix} -\rho \\ 0 \\ 0 \end{pmatrix} \tag{9}$$

By eqs 1, 4, and 7, the transformation matrix **N** is related to the matrix **A** as

$$\boldsymbol{N} = \boldsymbol{T}^{-1}\boldsymbol{A}\boldsymbol{T} \tag{10}$$

which confirms the *similarity* between the matrixes **N** and **A**. Thus, the trace of the matrix **N** coincides with the trace of the matrix **A**, i.e.

$$Tr[\boldsymbol{N}] = Tr[\boldsymbol{A}] \tag{11}$$

By eq 11, we can determine the relation between the pitch angle θ and the internal parameters.

We apply this treatment to the periodic polypeptide in which D- and L-amino acid residues are catenated alternately (DL-peptide). The DL-peptide includes three kinds of atoms (N, C^{α}, and C) in its backbone unit (Figure 1), and the adjacent units have a different chirality. Due to the enantiomeric relation of $\phi_L = -\phi_D$, $\psi_L = -\psi_D$, and $\omega_L = -\omega_D$, the orthogonal matrix $\mathbf{A}^{DL}$ for the DL-peptide is given using three orthogonal matrixes $\mathbf{A}_{\phi}$, $\mathbf{A}_{\psi}$, and $\mathbf{A}_{\omega}$, and also the transformation matrix **R** as follows

$$\boldsymbol{A}^{\mathbf{DL}} = \boldsymbol{A}_{\phi}\boldsymbol{A}_{\psi}\boldsymbol{A}_{\omega}\boldsymbol{R} \tag{12}$$

where

$$\boldsymbol{A}_{\phi} = \begin{pmatrix} -\cos\alpha_1 & -\sin\alpha_1 & 0 \\ \sin\alpha_1\cos\phi & -\cos\alpha_1\cos\phi & -\sin\phi \\ \sin\alpha_1\sin\phi & -\cos\alpha_1\sin\phi & \cos\phi \end{pmatrix} \tag{13}$$

$$\boldsymbol{A}_{\psi} = \begin{pmatrix} -\cos\alpha_2 & -\sin\alpha_2 & 0 \\ \sin\alpha_2\cos\psi & -\cos\alpha_2\cos\psi & -\sin\psi \\ \sin\alpha_2\sin\psi & -\cos\alpha_2\sin\psi & \cos\psi \end{pmatrix} \tag{14}$$

$$\boldsymbol{A}_{\omega} = \begin{pmatrix} -\cos\alpha_3 & -\sin\alpha_3 & 0 \\ \sin\alpha_3\cos\omega & -\cos\alpha_3\cos\omega & -\sin\omega \\ \sin\alpha_3\sin\omega & -\cos\alpha_3\sin\omega & \cos\omega \end{pmatrix} \tag{15}$$

and

$$\boldsymbol{R} = \begin{pmatrix} 1 & 0 & 0 \\ 0 & 1 & 0 \\ 0 & 0 & -1 \end{pmatrix} \tag{16}$$

Using the transformation matrix **R**, the orthogonal matrix $\mathbf{N}^{\mathrm{DL}}$ for the DL-peptide is also obtained as

$$\mathbf{N}^{\mathbf{DL}} = \mathbf{NR} = \begin{pmatrix} \cos\theta & -\sin\theta & 0 \\ \sin\theta & \cos\theta & 0 \\ 0 & 0 & -1 \end{pmatrix} \tag{17}$$

Because of the similarity between $\mathbf{A}^{\mathrm{DL}}$ and $\mathbf{N}^{\mathrm{DL}}$ ($Tr[\mathbf{A}^{\mathrm{DL}}] = Tr[\mathbf{N}^{\mathrm{DL}}]$), the pitch angle θ of the DL-peptide is expressed as a functional form of the internal parameters as follows

$$\cos\theta^{\mathrm{DL}} = \frac{1}{2}(a_{11}^{\mathrm{DL}} + a_{22}^{\mathrm{DL}} + a_{33}^{\mathrm{DL}} + 1) \tag{18}$$

where

$$a_{11}^{\mathrm{DL}} = \cos\alpha_3(\sin\alpha_1\sin\alpha_2\cos\psi - \cos\alpha_1\cos\alpha_2) + \sin\alpha_1\sin\alpha_3\sin\psi\sin\omega + \sin\alpha_3\cos\omega(\cos\alpha_1\sin\alpha_2 + \sin\alpha_1\cos\alpha_2\cos\psi) \tag{19}$$

$$a_{22}^{\mathrm{DL}} = \sin\alpha_3(\sin\alpha_1\cos\alpha_2\cos\phi + \sin\alpha_2\sin\phi\sin\psi + \cos\alpha_1\sin\alpha_2\cos\phi\cos\psi) + \cos\alpha_3\sin\omega(\sin\phi\cos\psi - \cos\alpha_1\cos\phi\sin\psi) + \cos\alpha_3\cos\omega(\sin\alpha_1\sin\alpha_2\cos\phi - \cos\alpha_2\sin\phi\sin\psi - \cos\alpha_1\cos\alpha_2\cos\phi\cos\psi) \tag{20}$$

$$a_{33}^{\mathrm{DL}} = \sin\omega(\cos\alpha_1\cos\alpha_2\sin\phi\cos\psi - \sin\alpha_1\sin\alpha_2\sin\phi - \cos\alpha_2\cos\phi\sin\psi) - \cos\omega(\cos\phi\cos\psi + \cos\alpha_1\sin\phi\sin\psi) \tag{21}$$

The pitch number *n* gives the number of residues per one helical turning, and this value is determined from the pitch angle θ by $n = 2\pi/\theta$. Thus, eqs 18−21 give the relation between *n* and the internal parameters α_i ($i = 1, 2, 3$), ϕ, ψ, and ω. In the following, we discuss the possible backbone conformations of the DL-peptide based on these equations.

B. Extended-Type and Bound-Type Backbones. Here, let us focus on the bond nature of the common polypeptide (Figure 1). The skeletal conformation of the polypeptide is dominantly determined by the internal rotation angles ϕ, ψ, and ω rather than the bond lengths r_i and the bond angles α_i, because r_i and α_i are hardly changed due to the peptides' covalent nature. Taking into account the above feature, we quote the following experimental values for r_i and α_i; $r_1 = 1.52$ Å, $r_2 = 1.33$ Å, $r_3 = 1.45$ Å, $\alpha_1 = 111°$, $\alpha_2 = 116°$, and $\alpha_3 = 122°$.[16,17] Moreover, we consider the flat amide plane of $\omega = 180°$ between C^{α} atoms, which is commonly found in the polypeptides unless they include any peculiar hydrogen bonds or steric hindrance in their own backbones. Under these assumptions, we can obtain the possible θ values (or *n* values, where $n = 2\pi/\theta$) with respect to two internal rotation angles ϕ and ψ. Thus, we can draw the three-dimensional (3D) plot of cos θ in terms of the two variables ϕ and ψ (Figure 3a), in accordance with eqs 18−21.

The periodic DL-peptide basically produces the *zero-transfer* helices (open rings) on the surface of cos θ (Figure 3a). The resulting minimum value of cos $\theta = 0.2588$ reveals that the available pitch number *n* is limited to more than 4.8. However, one should note that the possible *n* is further restricted to an even number so as to form the closed rings. Therefore, the minimum ring (residue) number is given as $n = 6$, i.e., an even number of $n = 6, 8, 10, 12, \ldots$ is available in the PCRs while maintaining the S_n symmetry.[14]

(15) Nakanishi, T. Thesis of Waseda University 2000.
(16) *Tables in Chemistry* (*Kagaku Binran* in Japanese), ed.; The Chemical Society of Japan: Maruzen, Tokyo, 1984.
(17) In section III, we also use those values as the initial values for the geometry optimization.

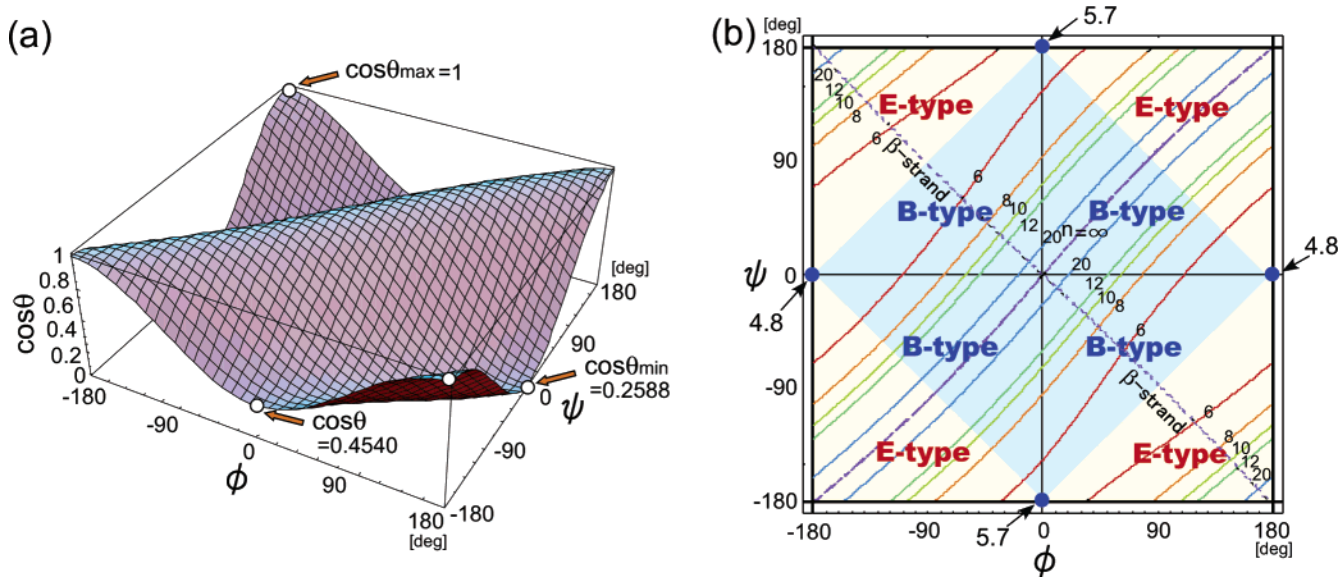

Figure 3. Possible cos θ values (a) and its *equi*-cos θ map (b) of the DL-peptide by varying the internal rotation angles ϕ and ψ. We give the pitch number n by integers on the solid lines in (b). On the dotted line of $\psi \simeq -\phi$, the β-strand type backbones are formed. In the calculation, we quote the following experimental values for the bond lengths and bond angles; $r_1 = 1.52$ Å, $r_2 = 1.33$ Å, $r_3 = 1.45$ Å, $\alpha_1 = 111°$, $\alpha_2 = 116°$, and $\alpha_3 = 122°$.[16] Moreover, we postulate the flat amide plane of $\omega = 180°$. If the three bond angles are the same ($\alpha_1 = \alpha_2 = \alpha_3$), these lines show a complete linearity. The actual polypeptide, however, causes a difference in these bond angles, and the nonlinear relation between ψ and ϕ is generated in the individual lines.

The possible PCR conformations are well understood by drawing the 2D contour map of cos θ (Figure 3b). The numerical values on the solid lines in Figure 3b correspond to the resulting pitch number n. The cosinodal dependence of ϕ and ψ included in eqs 19−21 causes four independent *equi-n* lines having the same n number. Those lines are respectively approximated by $\psi \simeq \phi + \pi \pm c$ and $\psi \simeq \phi - \pi \mp c$, where c is a constant defined by $0 < c < \pi$. Because those four lines have an inverse symmetry around the origin of $(\phi,\psi) = (0, 0)$, any two sets of (ϕ,ψ) having the above inverse symmetry produce an exactly equivalent backbone. Therefore, only in the meaning of determining the backbone conformation, can one reduce the variation region to half ($\psi > \phi$ or $\psi < \phi$).

An important result is that, even in the half region of $\psi > \phi$ or $\psi < \phi$, two *equi-n* lines appear for the individual n number. This result indicates that *two different backbone conformations are possible in the same n-residue PCR*. Those conformations are grouped into the bound-type (B-type) due to the internal rotation angles of $-\pi < \psi \pm \phi < \pi$, or the extended-type (E-type) in the other region (Figure 3b). The characteristic of these two conformations is that E-type PCRs have the conventional trans zigzag backbones, while the B-type PCRs have the new conformations whose skeletons are rather shrunk (Figure 4). These two types of the PCRs, thus, have a different internal diameter, i.e., the smaller B-type PCRs and the larger E-type PCRs.

Here, for the purpose of specifying the PCR conformation, we further narrow our discussion on such PCRs having their internal rotation angles (ϕ,ψ) of the crossing points between the individual solid line and the dotted line of $\psi \simeq -\phi$ (Figure 3b). The internal rotation angles on this dotted line provide the backbones whose skeletal planes are parallel to the ring axis. Therefore, the values of ϕ and ψ at these crossing points provide the PCR backbones of the β-strand type. Hereafter, we call these PCRs the *membered ring* (MR) forms. We show those *mathematical* E-type and B-type MRs of $n = 6$ in Figure 5, parts a and b, respectively. Because of the amide (O=C−N−H) being parallel to the ring axis, those MRs are supposed to construct tubular structures through inter-ring hydrogen bonds analogous to the β-sheets. The smaller diameter of the B-type MRs further excites our interest in the smaller B-type PNTs in addition to the conventional E-type PNTs.

III. Energetics of the Nanoring Backbones

The next subject is to investigate whether the above (*mathematical*) MR structures are energetically stable. For a quantitative discussion of the stable PCRs, we should investigate the energetics using parameter-free methods. Therefore, we carried out ab initio Hartree−Fock molecular orbital (MO) calculations by employing a *Gaussian98* program.[19] The normal vibrational analysis was also performed for the geometry optimization of the n-residue PCRs while maintaining the S_n symmetry. All of the calculations were carried out using the 6-31G** basis set for an intimate discussion of the hydrogen bonds.

A. Membered Rings. We will start from homo-Gly MRs having E-type and B-type backbones. The resulting relationship between the total energy (per residue) and the residue (pitch) number n is shown as the broken lines in Figure 6a. An important result is that the E-type MRs are more stable than the B-type MRs, independent of any n number. It is also characteristic that E-type MRs hardly change their own total energy,[20] although a significant energetic destabilization occurs in the B-type MRs with increasing n number. This destabilization in the B-type MRs is caused by the steric hindrance between

(18) Shimanouchi, T.; Mizushima, S. *Kagaku* **1947**, *17*, 24.
(19) Frisch, M. J.; Trucks, G. W.; Schlegel, H. B.; Scuseria, G. E.; Robb, M. A.; Cheeseman, J. R.; Zakrzewski, V. G.; Montgomery, J. A., Jr.; Stratmann, R. E.; Burant, J. C.; Dapprich, S.; Millam, J. M.; Daniels, A. D.; Kudin, K. N.; Strain, M. C.; Farkas, O.; Tomasi, J.; Barone, V.; Cossi, M.; Cammi, R.; Mennucci, B.; Pomelli, C.; Adamo, C.; Clifford, S.; Ochterski, J.; Petersson, G. A.; Ayala, P. Y.; Cui, Q.; Morokuma, K.; Malick, D. K.; Rabuck, A. D.; Raghavachari, K.; Foresman, J. B.; Cioslowski, J.; Ortiz, J. V.; Stefanov, B. B.; Liu, G.; Liashenko, A.; Piskorz, P.; Komaromi, I.; Gomperts, R.; Martin, R. L.; Fox, D. J.; Keith, T.; Al-Laham, M. A.; Peng, C. Y.; Nanayakkara, A.; Gonzalez, C.; Challacombe, M.; Gill, P. M. W.; Johnson, B. G.; Chen, W.; Wong, M. W.; Andres, J. L.; Head-Gordon, M.; Replogle, E. S.; Pople, J. A. *Gaussian 98*; Gaussian, Inc.: Pittsburgh, PA, 1998.

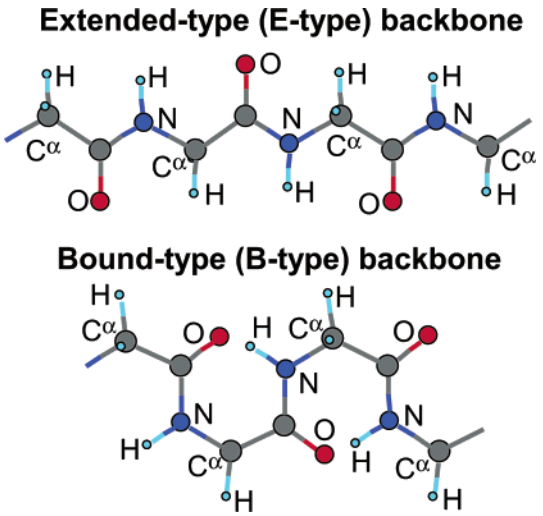

Figure 4. Illustration of the extended-type (E-type) peptide backbone and the bound-type (B-type) one.[18]

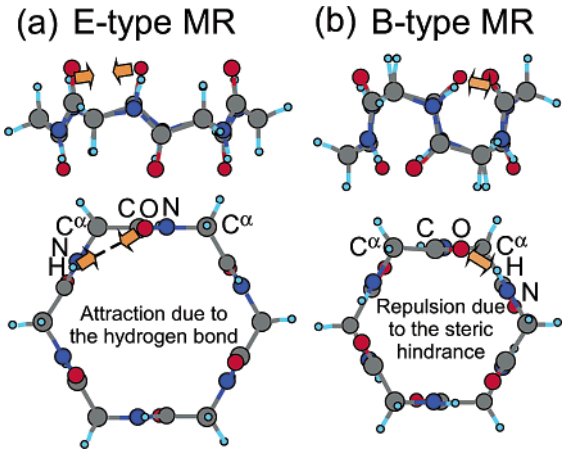

Figure 5. Side view and top view of the E-type MR (a) and B-type MR (b) consisting of six Gly residues. We assume that both backbones have amide planes of $\omega = 180°$. The intra-ring hydrogen bonds (HBs) cause an opposite role in E-type and B-type MRs; an attractive force occurs via HBs in the former, but a repulsive force exists in the latter due to the steric hindrance.

hydrogen (H) and oxygen (O) atoms located on the adjacent amide planes (Figure 5b). This feature is confirmed by the corresponding interatomic distance between H···O (Figure 6b), which reveals that the B-type MRs allow these two atoms to approach unrealistically, whereas the corresponding interatomic distance in the E-type MRs is still large enough to avoid steric hindrance.

B. Optimized Nanorings. The steric conformations of E-type and B-type MRs are changed by the geometry optimizations (Figure 7, parts a and b). The resulting internal rotation angles reveal that both E-type and B-type PCRs do not conserve the complete amide plane of $\omega = 180°$ (Table 1), and we cannot find the MR conformation anymore. Thus, we hereafter term these optimized PCRs as *novel ring* (NR) forms.

The characteristic feature found in the E-type NRs is that all three internal rotation angles deviate from those of the MR structure ($\psi \simeq \phi$ and $\omega = 180°$) with decreasing n number,

(20) With increasing n number, the skeletal backbones of E-type MRs approach that of the fully extended planar structure, which is the most energetically stable peptide skeleton.[10] Therefore, the total energy of the E-type MR slightly decreases with increasing n number.

Table 1. Internal Rotation Angles in the Optimized E-type and B-type Homo-Gly PCRs of $n = 6-12$ (RHF/6-31G**)[a]

	E-type			B-type		
n	ϕ (deg)	ψ (deg)	ω (deg)	ϕ (deg)	ψ (deg)	ω (deg)
6	−109.0	143.1	−170.1	83.8	−64.5	−175.3
8	−127.5	155.0	−172.3	83.9	−52.3	−164.2
10	−139.2	159.9	−174.1	83.0	−44.3	−158.4
12	−146.7	163.1	−175.2	81.9	−38.5	−155.0

[a] Although Gly has no chirality, we show the values corresponding to the L-amino acid residues of the *equatorial* substitution (Figure 9a).

i.e., the ω value deviates from (−)180° and the remaining two angles deviate from $\psi \simeq -\phi$ (Table 1). This characteristic is caused by the intra-ring hydrogen bond (HB) of N−H···O induced by the cyclization of the peptide chain (Figure 8a). This feature is also confirmed by the reduction of the interatomic H···O distance from the E-type MR to the E-type NR (Figure 6b) and by an increase in the overlap population between H···O (by 55%).

In the B-type PCRs, on the other hand, the H···O distance is so shortened that significant steric hindrance occurs with increasing n number if the backbones maintain the MR forms (Figure 6b). The H···O distance is therefore elongated to about 2.0 Å, independent of the n number (Figure 6b). When n is small, only a small structural change is required so as to relax the steric hindrance. Thus, we can find only a slight ω deviation in the B-type NR of $n = 6$ (Table 1). On the contrary, the relaxation of the steric hindrance further requires a large ω deviation when $n \geq 8$. Therefore, the amide plane is gradually distorted with the increasing n number.

A noticeable point is that the relaxation energy in the B-type PCRs overcomes the stabilization energy in the E-type PCRs (Figure 6a). As a result, the total energies of E-type NRs and B-type NRs become comparable. By focusing on the resulting energy difference, we can find that the smaller rings prefer the novel B-type backbone, while the larger rings prefer the conventional E-type backbone: When $n \geq 10$, the E-type NRs are still more stable than the B-type NRs. However, at a small n of $n \leq 8$, the B-type NRs become more stable than the E-type NRs.

IV. Substitution of Amino Acid Residues

We also investigate the stable molecular conformations of the PCRs whose amino acid residues are replaced homogeneously by one of 20 encoded amino acids (homo-residue PCRs). Although two types of substitution means are presumable (the *equatorial* substitution and the *axial* substitution;[21] in Figure 9, parts a and b), we limit our discussion to only the *equatorial* substitution, because the *axial* substitution is considered to prevent its own stacking due to the repulsion between the side chains of the adjacent PCRs. Also the geometry optimization was carried out for the smallest six-residue PCRs using the 6-31G** basis set while maintaining the S_6 symmetry.

A. Molecular Structures and Energetics. One of the important results given by the present calculations is that all kinds of homo-residue PCRs have both the extended-type (E-type) and the bound-type (B-type) backbones as their local

(21) For E-type PCRs, the *equatorial* substitution appears in the region of $\psi > \phi + \pi$, and the *axial* substitution appears in the region of $\psi < \phi - \pi$ (Figure 3b). For B-type PCRs, on the other hand, the *equatorial* substitution appears in the region of $\phi - \pi < \psi < \phi$, and the *axial* substitution appears in the region of $\phi < \psi < \phi + \pi$.

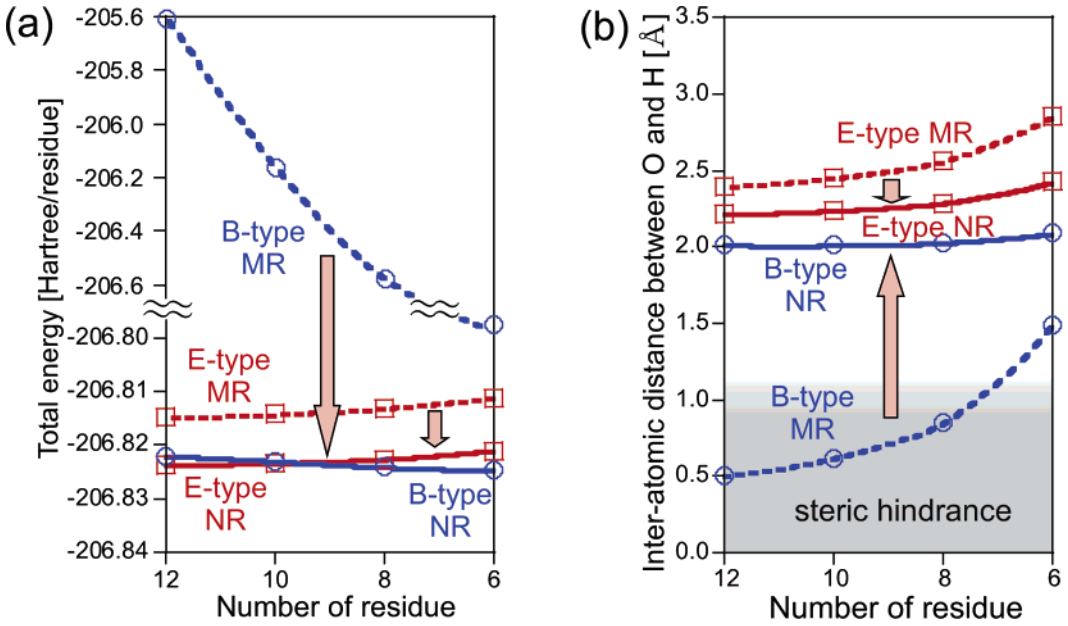

Figure 6. Relationship between the calculated total energy (per residue) and the residue (pitch) number n (a), and that between the interatomic H···O distance of the intra-ring N−H···O and n in the E-type and B-type PCRs (b). In both figures, we show these relations for the four PCRs of the MRs (broken lines) and the optimized NRs (solid lines), respectively. We also depict the region of the steric hindrance by the gray tone.

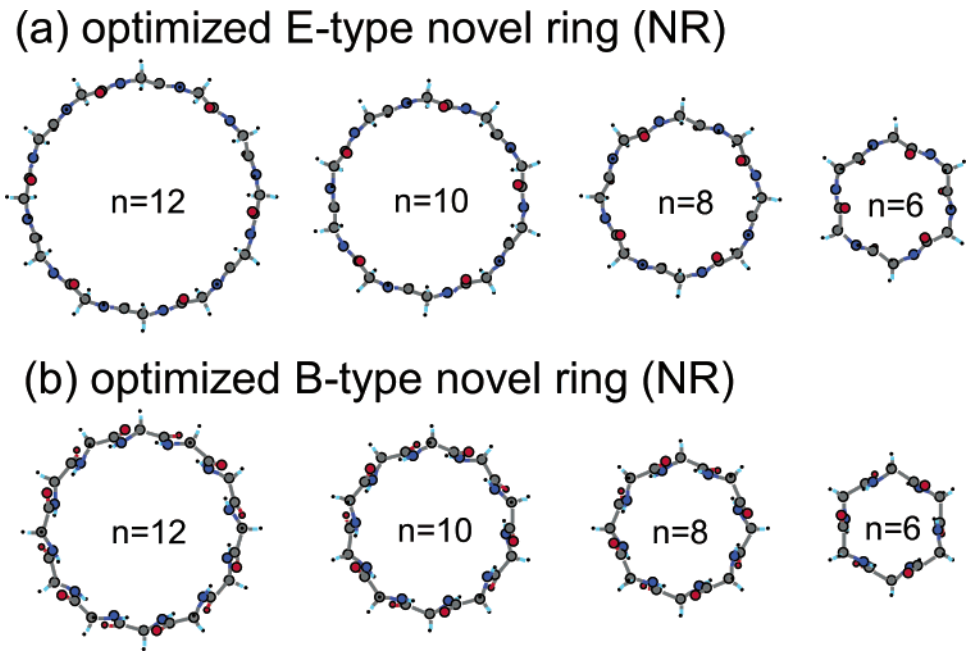

Figure 7. Optimized molecular structures of the E-type PCRs (a) and B-type PCRs (b) consisting of 12, 10, 8, and 6 Gly residues.

minimum forms. Moreover, the substitution of the amino acid residues hardly changes the bond lengths and the bond angles of the PCR backbones; The resulting bond lengths are changed at most by ±1%, and the bond angles are within ±4%. The detailed structural difference, therefore, appears through the internal rotation angles ϕ, ψ, and ω. The resulting internal rotation angles are listed in Table 2.[22]

The global minimum form of the individual homo-residue PCR is determined by an energy comparison between the E-type and B-type PCRs. The present result reveals that the preferable backbone type is not unique but depends on the individual amino acid side chains even with the same number (n) of residues (Figure 10): The resulting energy difference indicates that seven residues of Gln, Cys, Tyr, Phe, Gly, Thr, and Ser prefer the B-type backbone, whereas the remainder prefer the E-type backbone.

Among all of the 20 encoded amino acid residues, five residues of Pro, Trp, Asp, Asn, and His appreciably prefer the E-type backbone by more than 1.5 kcal/mol per residue[23] (Figure 10). Therefore, those residues are expected to produce E-type

(22) Although the side chains have a large number of degrees of freedom, we determined the initial side-chain conformation to be $\chi_1 = -120°$ and $\chi_i = 180°$. This initial structure lets the normal vector of the side-chain plane be perpendicular to the S_6 axis. The PCR geometry was then optimized while maintaining the S_6 symmetry. As a result, one of three rotamer types (gauche(+), gauche(−), or trans) was obtained for the individual homo-residue PCR as the local minimum structure. The resulting χ_1 angles and rotamer type are also listed in Table 2. The PCRs might also have the other rotamer types for the local minimum forms. However, the other rotamer types are out of consideration in the present paper because of the large number of degrees of freedom in the calculations.

Table 2. Internal Rotation Angles in 20 Kinds of Homo-Residue PCRs Having E-type and B-type Conformations (RHF/6-31G**)

	E-type					B-type				
residue	ϕ (deg)	ψ (deg)	ω (deg)	χ_1 (deg)[a]	rotamer type[b]	ϕ (deg)	ψ (deg)	ω (deg)	χ_1 (deg)[a]	rotamer type[b]
Pro	−75.3	128.9	171.8	31.8	gauche(−)	49.2	−0.8	−137.9	−22.5	gauche(+)
Trp	−118.0	134.3	−173.8	−69.1	gauche(+)	75.3	−58.5	−177.4	−64.3	gauche(+)
Asp	−143.8	108.2	180.0	−177.0	trans	75.6	−59.8	−177.5	−66.1	gauche(+)
Asn	−145.1	106.1	179.4	−176.5	trans	78.6	−60.1	−176.2	−55.2	gauche(+)
His	−131.6	120.6	−177.0	−176.5	trans	75.0	−64.8	−176.7	−178.2	trans
Met	−119.6	136.7	−171.1	−64.5	gauche(+)	73.7	−60.5	−178.2	−61.4	gauche(+)
Glu	−119.7	138.3	−169.7	−63.2	gauche(+)	73.8	−60.5	−178.2	−60.7	gauche(+)
Lys	−129.3	126.8	−174.1	−176.8	trans	74.5	−61.3	−177.4	−170.7	trans
Arg	−128.4	126.3	−174.8	−177.0	trans	74.6	−61.0	−177.2	−170.2	trans
Val	−129.3	134.1	−168.3	−177.1	gauche(+)[c]	71.8	−54.4	−180.0	−177.5	gauche(+)[c]
Ile	−127.4	134.2	−169.5	−66.4	gauche(+)	72.1	−55.1	−179.4	−59.9	gauche(+)
Leu	−128.2	126.4	−175.0	−179.1	trans	73.7	−60.7	−177.8	−175.7	trans
Ala[d]	−121.5	133.1	−172.9			74.7	−60.6	−177.7		
Gln	−124.9	127.0	−176.1	−179.1	trans	74.9	−61.2	−177.4	−58.5	gauche(+)
Cys	−110.0	134.2	−176.8	−61.6	gauche(+)	75.5	−61.9	−177.1	−58.6	gauche(+)
Tyr	−117.2	130.8	−176.5	−60.7	gauche(+)	76.3	−59.2	−177.2	−57.4	gauche(+)
Phe	−116.2	131.1	−176.6	−61.2	gauche(+)	76.2	−59.4	−177.2	−57.7	gauche(+)
Gly[d]	−109.0	143.1	−170.1			83.8	−64.5	−175.3		
Thr	−97.2	162.1	−161.0	−62.6	gauche(+)	76.5	−45.0	−179.2	−47.1	gauche(+)
Ser	−92.5	163.7	−162.4	60.8	gauche(−)	80.3	−47.4	−178.5	85.0	gauche(−)

[a] χ_1 is a dihedral angle of N−Cα−Cβ−Cγ in the side chain. [b] The rotamer types of the side chains are classified into the following three groups; gauche(+) defined by $\chi_1 = -60° \pm 60°$, gauche(−) defined by $\chi_1 = +60° \pm 60°$, and trans defined by $\chi_1 = 180° \pm 60°$. [c] Val has a different convention for rotamers: gauche(−) is $-60° \pm 60°$, trans is $+60° \pm 60°$, and gauche(+) is $180° \pm 60°$. [d] Ala and Gly do not have Cγ atom.

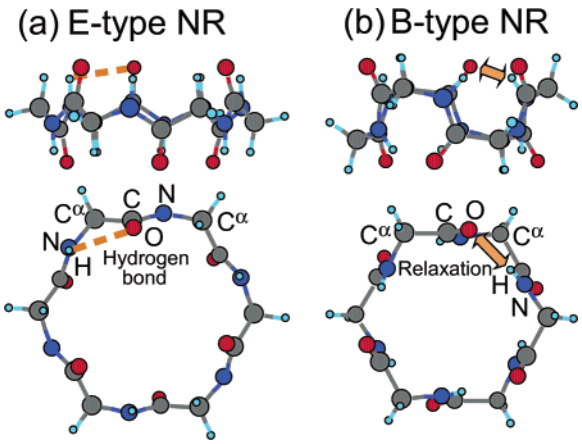

Figure 8. Side view and top view of the E-type (optimized) NR (a) and the B-type (optimized) NR (b) consisting of six Gly residues.

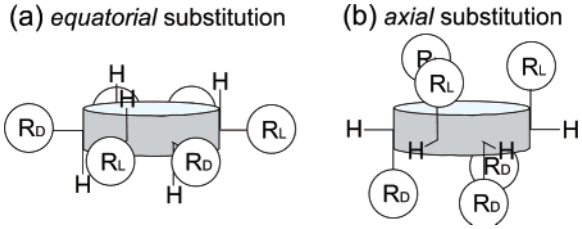

Figure 9. Illustration of the *equatorial* substitution (a) and the *axial* substitution (b). In the *equatorial* substitution, the replaced side chains are settled on the outside of the ring skeleton, whereas the side chains in the *axial* substitution are arranged toward the ring axis.

PCRs predominantly (E-forming residues). On the contrary, Gly, Thr, and Ser rather prefer the B-type backbone by more than 2 kcal/mol per residue. Thus, those three residues are supposed to be B-forming ones. An interesting point is that the remaining homo-residue PCRs of Met, Glu, Lys, Arg, Val, Ile, Leu, Ala, Gln, Cys, Tyr, and Phe show a small and indistinguishable energy difference (within 1 kcal/mol per residue). Therefore, those residues have a potential to produce both E-type and B-type PCRs (E/B-forming residues). We illustrate the energetically preferable molecular conformations of 20 homo-residue PCRs in Figure 11.

B. Interaction between the Side Chains and the Backbone. The resulting energetics is basically understood by the presence or absence of the hydrogen bonding interaction between the side chains and the backbone. One of the examples is the replacement by Asp and Asn, which belong to E-forming residues. The replacement by those residues induces the hydrogen bond (HB) of O···H−N between the side-chain O atom and the backbone H−N bond (Figure 12). This HB functions effectively in the E-type PCRs but not in the B-type PCRs. The reason is that the B-type backbone has an undesirable N−H bond inclined against the ring axis, and therefore, the O···H distance is more elongated than that in the E-type PCRs by 13%. Because of this characteristic, those residues appreciably prefer the E-type backbone to the B-type backbone[24] (Figure 10).

On the contrary, homo-residue PCRs of Thr and Ser include the HB only in the B-type conformation but not in the E-type conformation (Figure 12), in contrast to the PCRs of Asp and Asn. This opposite feature is caused by the difference in the HB nature. HBs in the homo-residue PCRs of Thr and Ser are those O−H···O between the side-chain O−H bond and the backbone O atom. Therefore, in the B-type conformation, the backbone C═O bond is so oriented toward the side chain that the HB of O−H···O is induced and points the side-chain O−H bond toward the backbone. In the E-type conformation, on the contrary, the backbone C═O bond is not oriented toward the side chains but toward the ring axis. Therefore, it is hard to produce the HB (O−H···O) between the side-chain O−H bond and the backbone O atom (Figure 12). Because of this

(23) Only the homo-Pro PCR shows a considerably large energetic stability in the E-type conformation (by 20.6 kcal/mol per residue). This is because the peculiar atomic loop included in the Pro residue generates the large backbone distortion especially in the B-type conformation as shown in Table 2.

(24) Homo-residue PCRs of Trp and His also show the large energetic stability in the E-type conformation, despite the fact that they include no HB between the side chains and the backbone.

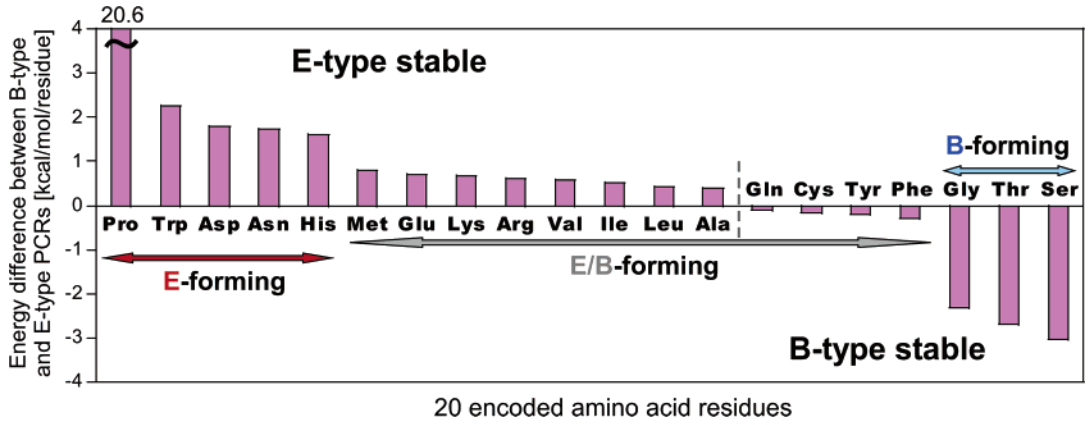

Figure 10. Total energy differences between E-type and B-type PCRs with respect to the replaced amino acid residues. A positive value means that the E-type PCR is more stable than the B-type PCR, whereas a negative value means the opposite.

characteristic, Thr and Ser prefer the B-type backbone to the E-type backbone (Figure 10).

The replacement by the remaining E/B-forming residues does not produce any plain HBs between the side chains and the backbone (Figure 12). Therefore, homo-residue PCRs of those residues do not show a prominent energetic stability in either the E-type or the B-type. However here, one should remember that the PCR backbone itself (homo-Gly PCR) rather prefers the B-type conformation without HBs between the side chains and the backbone (when $n = 6$). Thus, we can also conclude that the substitution of the amino acid residues tends to enhance the energetic stability of the E-type PCRs compared with that of the B-type PCRs (Figure 10).

C. Electronic Structures. In this section, we discuss the electronic structures of homo-residue PCRs. Let us first focus on the simplest homo-Gly PCRs (PCR backbones). The resulting electronic structure of the E-type backbone is similar to that of the B-type backbone (Figure 13, parts a and b). In both types of PCRs, the highest occupied molecular orbital (HOMO) and the lowest unoccupied molecular orbital (LUMO) are formed by the backbone π states whose orbital lobes are in the ring plane (in-plane) as shown in the figure.

The substitution of the amino acid residues inserts additional energy levels into the electronic structure of the PCR backbone (Figure 14, parts a−c). A noticeable point is that the intruded levels around the HOMO or LUMO are well localized at the replaced side chains, i.e., no orbital mixing occurs between the side chains and the backbone. Moreover, the HB interactions between the side chains and the backbone (O···H−N and O−H···O) do not hybridize with the intruded states and also with the frontier π states due to the orthogonality between the π states and H 1*s* orbitals. Thus, the electronic structures of homo-residue PCRs cannot be classified based on the energetics but be classified based on the substituent groups.

The resulting electronic structures of homo-residue PCRs are classified into the following three groups: In the first group (Group I), the energy levels of the side chains are buried in the valence states or the conduction states (Figure 14a). Those intruded levels are nearly 6-fold degenerated, because the neighboring side chains are so apart that those side chains do not interact mutually. This type of electronic structure is found in the homo-residue PCRs of Pro and Asn of the E-forming residues and of Val, Ile, Leu, Ala, and Gln of the E/B-forming residues.

Another type of the electronic structures is classified as Group II, in which the localized state originating from side-chain oxygen (O), nitrogen (N), or sulfur (S) appears at the top of the valence state[25] (Figure 14b). This type of electronic structure is found in homo-residue PCRs of Asp (E-forming residue), of Met, Glu, Lys, Arg, and Cys (E/B-forming residues) and of Thr and Ser (B-forming residues). In the homo-residue PCRs of Asp, Glu, Thr, and Ser, the on-site energy of the O 2p state appears just below the HOMO being nearly 6-fold degenerated (Figure 14b). However, when the component residues are replaced by Lys or Arg, the on-site levels are lifted and intruded into the energy gap due to the higher energy of the N 2p state (Figure 14b). Those fully occupied levels are furthermore pulled upward in the PCRs of Met or Cys, which includes a sulfur atom having a much higher on-site energy (Figure 14b).

The replacement by the remaining residues (Trp, His, Tyr, and Phe) provides the other type of electronic structure (Group III), in which both the upper valence state and the lower conduction state are modified by the side-chain π electrons (Figure 14c). The number of the intruded π states is uniquely determined by the atomicity of the membered ring in the replaced side chains. When the side chains include the six-membered ring (in Phe), six π states appear in the electronic structure while maintaining the individual π states nearly 6-fold degenerated (Figure 14c). Among those π states, quasi-degenerated π and π^* levels[26] are intruded into the energy gap and form the highest occupied state and the lowest unoccupied state, respectively. Moreover, the resolution of these quasi-degenerated energy is enhanced in the homo-Tyr PCR because of the symmetry lowering by an additional oxygen atom (Figure 15a).

In homo-His PCR, on the other hand, five π states appear in the electronic structure due to the five-membered ring of the side chain (Figure 15b). Because the membered ring includes nitrogen atoms, the resolution of the quasi-degenerated energy is further enhanced. However, two occupied π levels are still within the energy gap while maintaining the individual π states being 6-fold degenerated (Figure 15b). On the contrary, two unoccupied π^* levels are both crowded out of the energy gap and buried in the conduction states. In consequence, the lowest unoccupied state is formed by the backbone state, whereas the

(25) Takeda, K.; Shiraishi, K. *J. Phys. Soc. Jpn.* **1996**, *65*, 421.
(26) These π states do not degenerate completely because the point group symmetry of Phe is reduced from the D_{6h} symmetry of benzene due to the connection of a C^{β} atom. However, the individual π levels still maintain the 6-fold degeneracy.

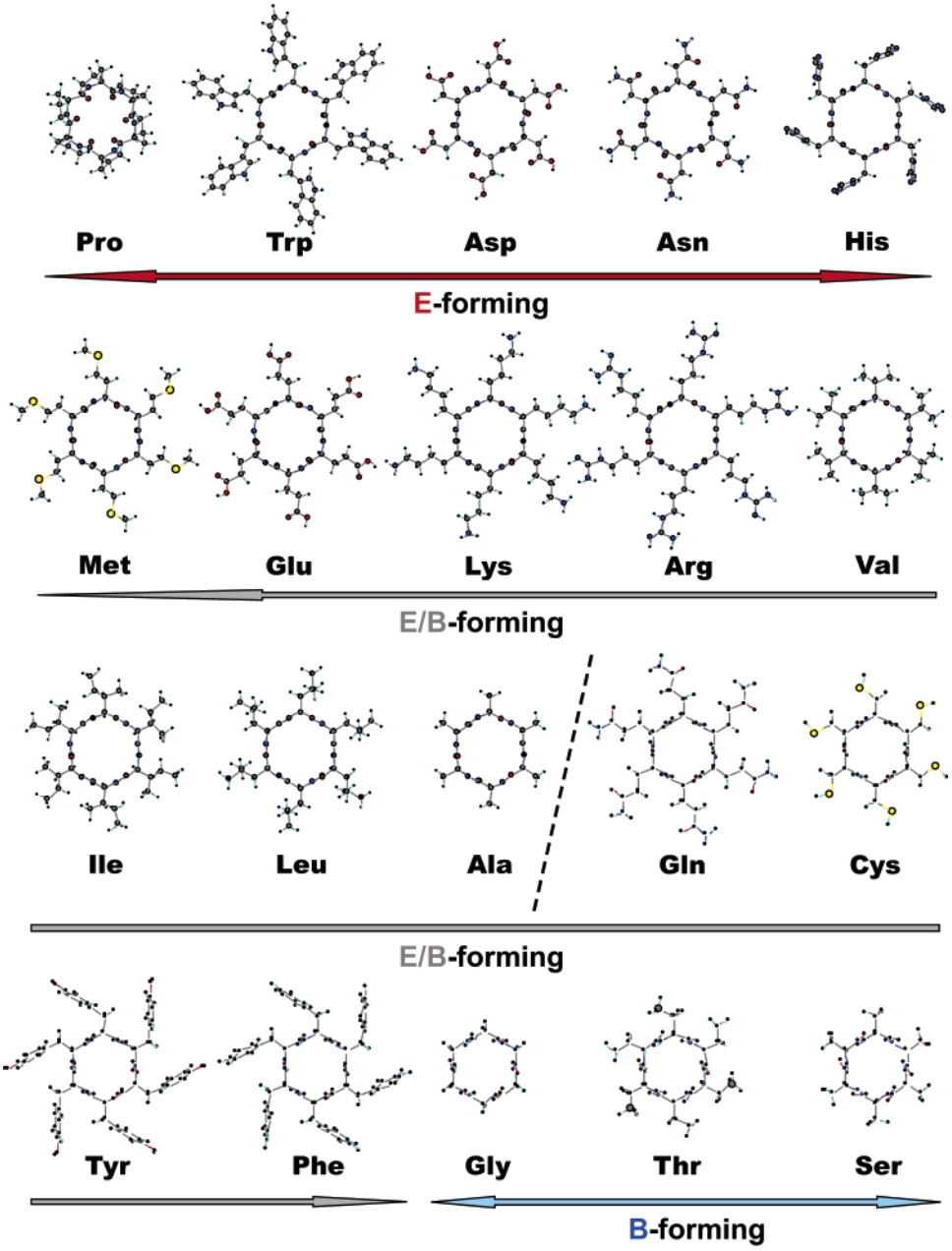

Figure 11. Optimized molecular structures of 20 homo-residue PCRs, in which the amino acid side chains locate the *equatorial* position. We illustrate the energetically preferable backbone type in the figure.

highest occupied state is still formed by the side-chain π orbital.[27]

If the component residues are replaced by Trp having a five- and six-membered ring, nine π states are embedded in the electronic structure (Figure 15c). Among those π states, three π levels and one π^* level appear in the energy gap, and therefore, the frontier orbitals of the homo-Trp PCRs are both formed by the side-chain π states in the present calculation. All of the above results indicate that the membered ring forms in the side chains are expected to be a certain reaction site in the PCRs and also in the other peptide systems.

V. Peptide Nanotubes

How do the PCRs stack to form the peptide nanotubes (PNTs)? In this section, we discuss the electronic and molecular structures of the PNT backbone. Because one can prospect two kinds of the PCR stacking means of parallel and antiparallel, we consider the following four types of PNTs: One is the PNT in which E-type PCRs are stacked parallel (E-type parallel PNT). The remainder are those PNTs of E-type antiparallel, B-type parallel, and B-type antiparallel. For these four types of the PNTs, we carried out Hartree−Fock energy calculations.

The geometry optimization and total energy calculations were carried out as follows: We start to obtain an optimal inter-ring

(27) This characteristic is well understood using the Hückel approach. If the membered ring of $(CH)_m$ consists of six atoms ($m = 6$), then the energy value of the degenerated π and π^* levels is given by $E_\pi = \alpha + \beta$ and $E_{\pi^*} = \alpha - \beta$, respectively.[28] However, those levels are lifted to be $E_\pi = \alpha + 0.62\beta$ and $E_{\pi^*} = \alpha - 1.62\beta$ when the atomicity of the membered ring is changed to $m = 5$ as illustrated in Figure 15. Therefore, the π^* levels are put into the conduction band, while the π levels are still within the energy gap.

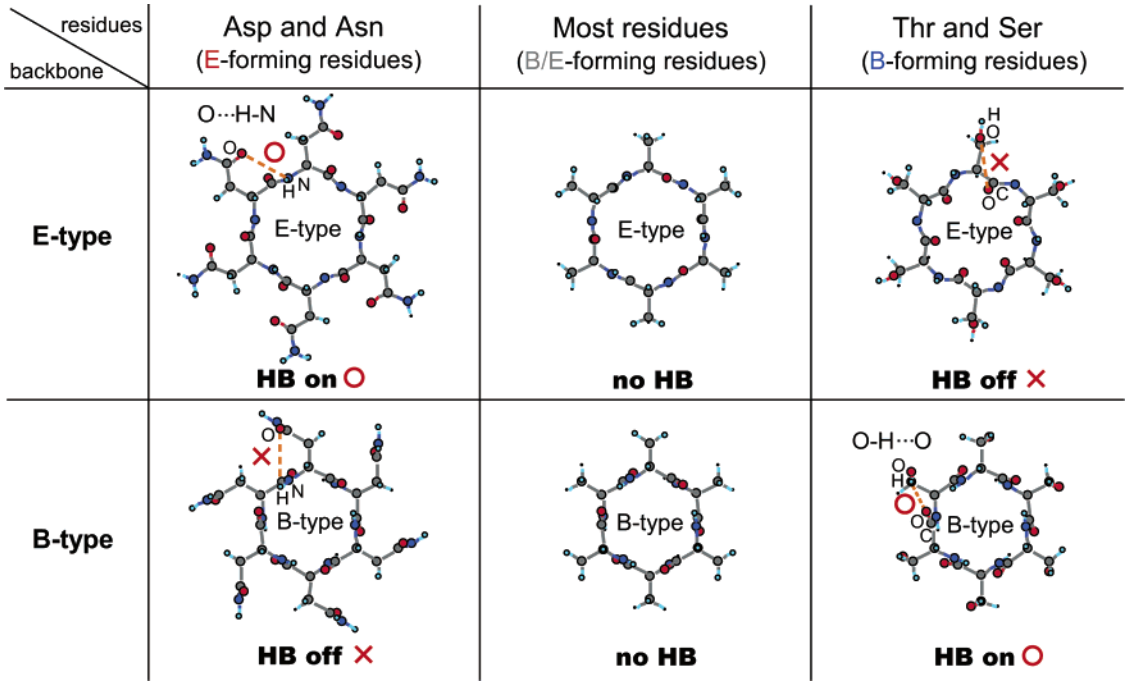

Figure 12. Three groups of the molecular structures in homo-residue PCRs. The replacement by Asp and Asn, which belong to E-forming residues, induces the hydrogen bond (HB) of O···H−N between the side-chain O atom and the backbone H−N bond in the E-type conformation, but not in the B-type one. On the contrary, the replacement by Thr and Ser, which belong to B-forming residues, produces the HB of O−H···O between the side-chain O−H bond and the backbone O atom in the B-type PCR, but not in the E-type PCR. The replacement by the E/B-forming residues does not cause any HBs between the side chains and the backbone in neither the E-type nor the B-type. We illustrate the homo-residue PCRs of Asn, Ala, and Ser on behalf of those three groups of molecular structures, respectively.

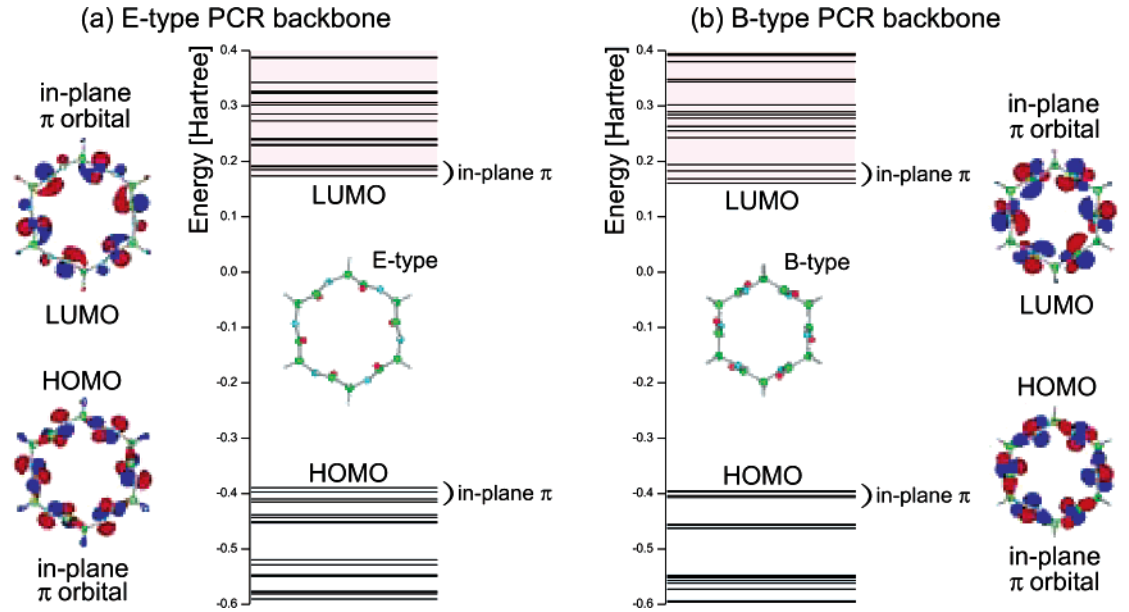

Figure 13. Electronic structure of the E-type PCR (a) and the B-type PCR (b) consisting of six Gly residues (RHF/6-31G**). The highest occupied molecular orbital (HOMO) and the lowest unoccupied molecular orbital (LUMO) are also illustrated.

distance using the model tube constructed by stacking three NRs parallel or antiparallel. After the inter-ring optimization, the molecular structure of three rings is fully optimized by freezing the above inter-ring distance. We next pick out the center ring and reform the PNT by stacking these rings. We then recalculate the optimal inter-ring distance. Finally, at this re-optimized inter-ring distance, we fully optimize the molecular structure of the three rings and determine the "optimized" PNT unit by picking out the center ring. The change in the resulting total energy is then calculated by varying the inter-ring distance in these "optimized" PNTs. In the geometry optimization, we consider the PNTs formed by the stacking of the smallest PCRs consisting of six Gly residues.

A. Optimized Molecular Structures. First, let us discuss the molecular structures of the E-type PNTs. The optimized backbone conformations of the E-type parallel and E-type antiparallel PNT are shown in Figure 16, parts a and b. The resulting internal rotation angles reveal that the PCR unit of the parallel PNT is similar to that of the antiparallel PNT (Table 3). In both PNTs, the ω angle approaches (−)180°, and

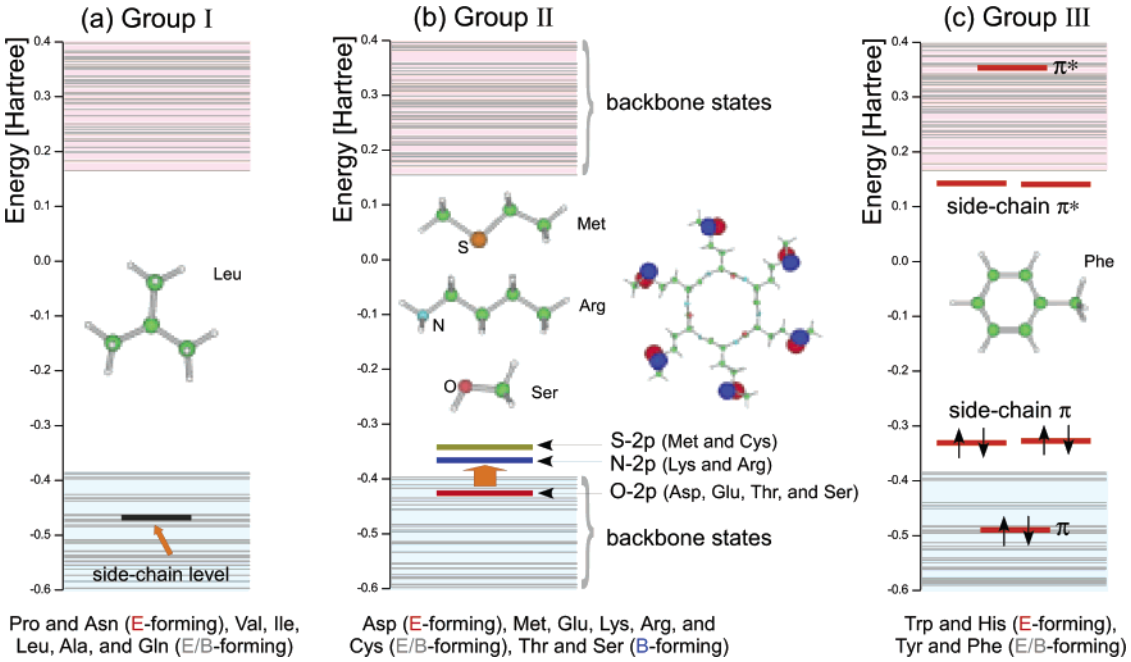

Figure 14. Three types of the electronic structures in homo-residue PCRs. The electronic structure of Group I, in which the energy levels of the side chains are buried in the valence states or the conduction states (a). Homo-residue PCRs of Pro and Asn (E-forming residues) and of Val, Ile, Leu, Ala, and Gln (E/B-forming residues) have this type of electronic structure. The electronic structure of Group II, in which the on-site energy of oxygen (O), nitrogen (N), or sulfur (S) appears at the top of the valence state (b). This type is found in the homo-residue PCRs of Asp (E-forming residue), of Met, Glu, Lys, Arg, and Cys (E/B-forming residues) and of Thr and Ser (B-forming residues). The electronic structure of Group III, in which the side-chain π electrons modify the upper valence state and the lower conduction state (c). Homo-residue PCRs of Trp, His, Tyr, and Phe have this type of electronic structure. All those intruded levels are nearly 6-fold degenerated, respectively. We illustrate the electronic structure of the E-type homo-Leu PCR (a), the E-type homo-Met PCR (b), and the B-type homo-Phe PCR (c) on behalf of those three types of electronic structure. We also show the change in the on-site energy in (b).

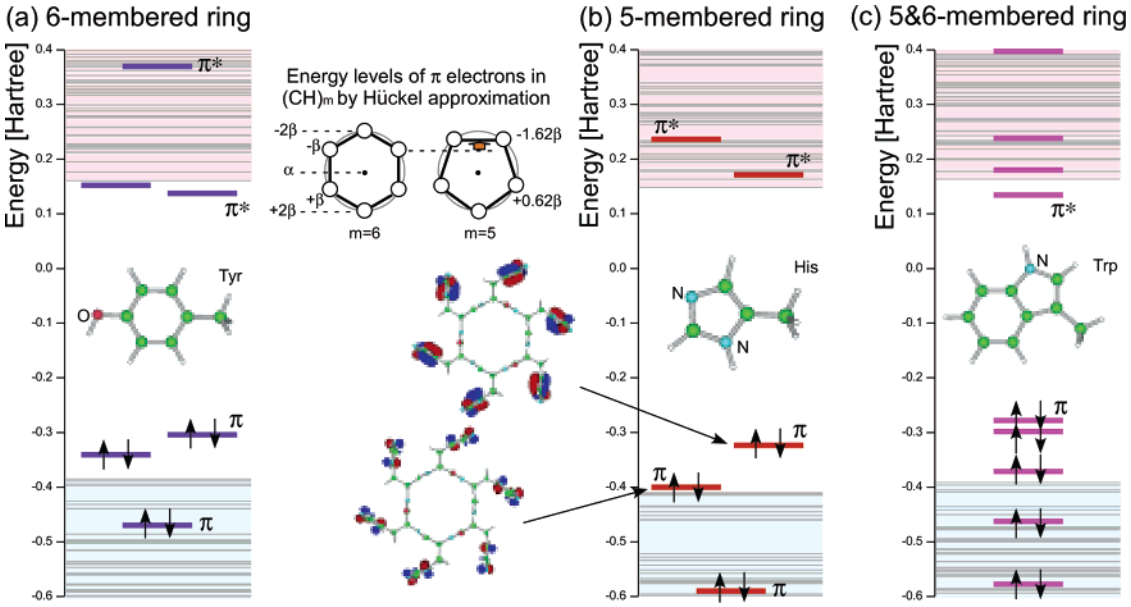

Figure 15. Change in the intruded π states of Group III homo-PCRs. The electronic structure of the E-type PCR of Tyr, His, and Trp is shown in (a), (b), and (c), respectively. One should remember that all the intruded π states are nearly 6-fold degenerated.

the remaining two angles are close to $\psi \simeq -\phi$. This feature makes the backbone conformation revert to the (initial *mathematical*) MR form. The present calculations also provide the similar inter-ring distances of 4.90 Å for the E-type parallel PNT and 4.95 Å for the E-type antiparallel PNT.

The conformation change from the isolated PCR to the PNT is caused by the inter-ring hydrogen bonds (HBs) of N−H···O and C^{α}−H···O (in Figure 16, parts a and b). In the E-type parallel PNT, the H···O distance of N−H···O is reduced to 2.0 Å and that of C^{α}−H···O is 2.5 Å. As a result, the overlap populations of those inter-ring HBs increase to overcome the intra-ring HB. This is the reason the optimized backbone reverts to the MR form. However, the complete amide plane of $\omega = 180°$ is not reproduced because the intra-ring HB is still alive in the PNT. The same feature is also found in the antiparallel PNT.

The structural difference between the parallel and the antiparallel PNT is that the former has a monotonic stacking form

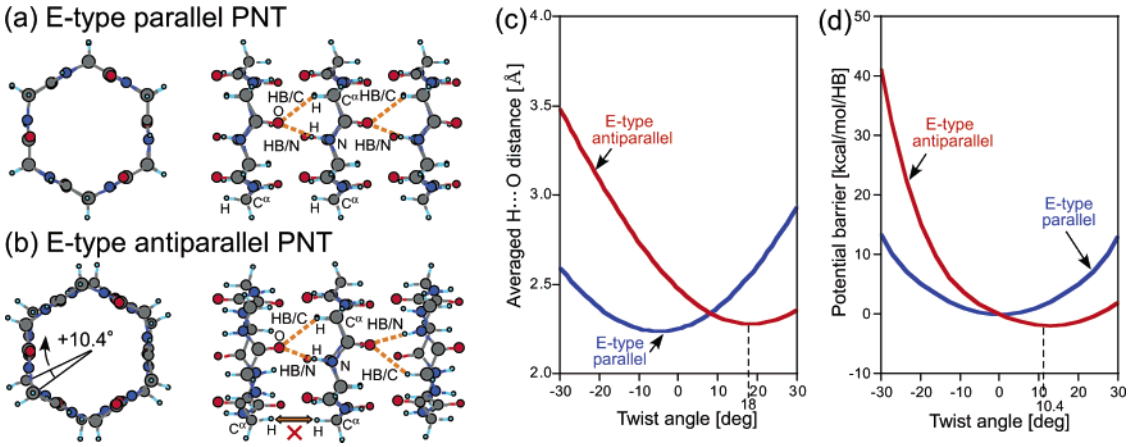

Figure 16. Top view and side view of the optimized molecular structure of the E-type parallel PNT (a) and E-type antiparallel PNT (b). In the antiparallel stacking, the individual PCRs are twisted alternately by 10.4°. We also show the averaged H···O distance of N−H···O and Cα−H···O (c), and the potential barrier (d) by varying the twist angle between the adjacent PCRs. The vertical line in (d) shows the energy difference from 0°.

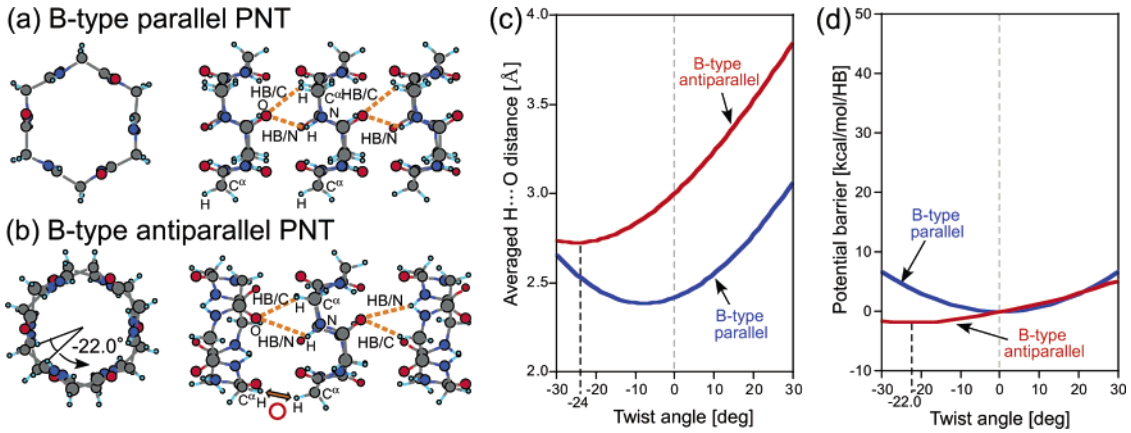

Figure 17. Top view and side view of the optimized molecular structure of the B-type parallel PNT (a) and the B-type antiparallel PNT (b). In the antiparallel stacking, the individual PCRs are twisted alternately by 22.0°. We also show the averaged H···O distance of N−H···O and Cα−H···O (c), and the potential barrier (d) by varying the twist angle between the adjacent PCRs. The vertical line in (d) shows the energy difference from 0°.

Table 3. Internal Rotation Angles in the PCR Units of E-type Parallel, E-type Antiparallel, B-type Parallel, and B-type Antiparallel PNTs (RHF/6-31G**)

stacking	E-type			B-type		
mean	ϕ (deg)	ψ (deg)	ω (deg)	ϕ (deg)	ψ (deg)	ω (deg)
parallel	−119.2	124.1	−177.5	90.9	−78.5	−172.4
antiparallel	−119.5	125.0	−177.0	86.7	−67.3	−173.9

(Figure 16a), whereas the latter provides a twisted PNT form, i.e., the adjacent PCRs are rotated alternately (Figure 16b). This feature is caused by the competition between the two inter-ring HBs of N−H···O and Cα−H···O. The parallel stacking gives the minimum H···O distance when the twist angle is around 0° (Figure 16c). On the contrary, in the antiparallel stacking, the minimum H···O distance is found when the twist angle is +18° (Figure 16c). Thus, the PCRs are rotated in the E-type antiparallel PNT by 10.4° (Figure 16d).

B-type PNTs also show a similar twisted nature in the antiparallel stacking (Figure 17b), although the parallel stacking of the B-type PCRs provides a monotonic stacking form (Figure 17a). The corresponding twist angle of 22.0° (Figure 17d) is well understood by the fact that the antiparallel stacking of the B-type PCRs gives the minimum H···O distance at −24° (Figure 17c). One should also notice that the negative value of the twist angle indicates that the B-type PCRs are rotated in the opposite direction compared with the E-type PCRs.

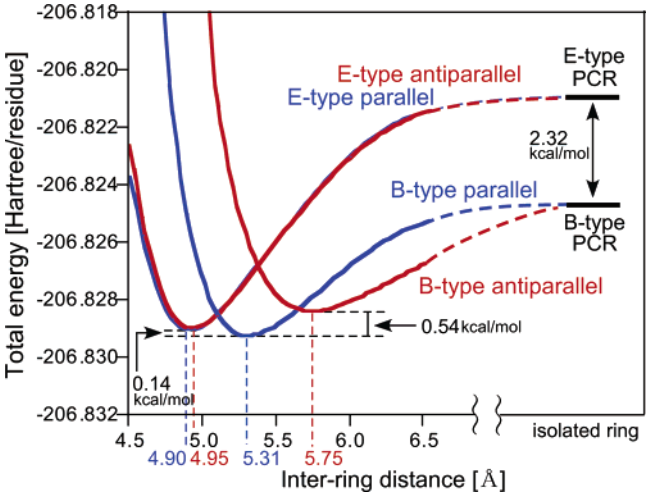

Figure 18. Relationship between the total energy (per residue) and the inter-ring distances in the PNTs.

The optimal inter-ring distances in the B-type PNTs are rather different between parallel and antiparallel stacking. While the B-type parallel PNT has a value of 5.31 Å, the antiparallel PNT provides a larger inter-ring distance of 5.75 Å (Figure 18). This feature is caused by the inter-ring repulsion of Cα−H···H−Cα. Although the parallel PNT has no overt repulsion, the B-type antiparallel PNT includes a slight Cα−H···H−Cα repulsion

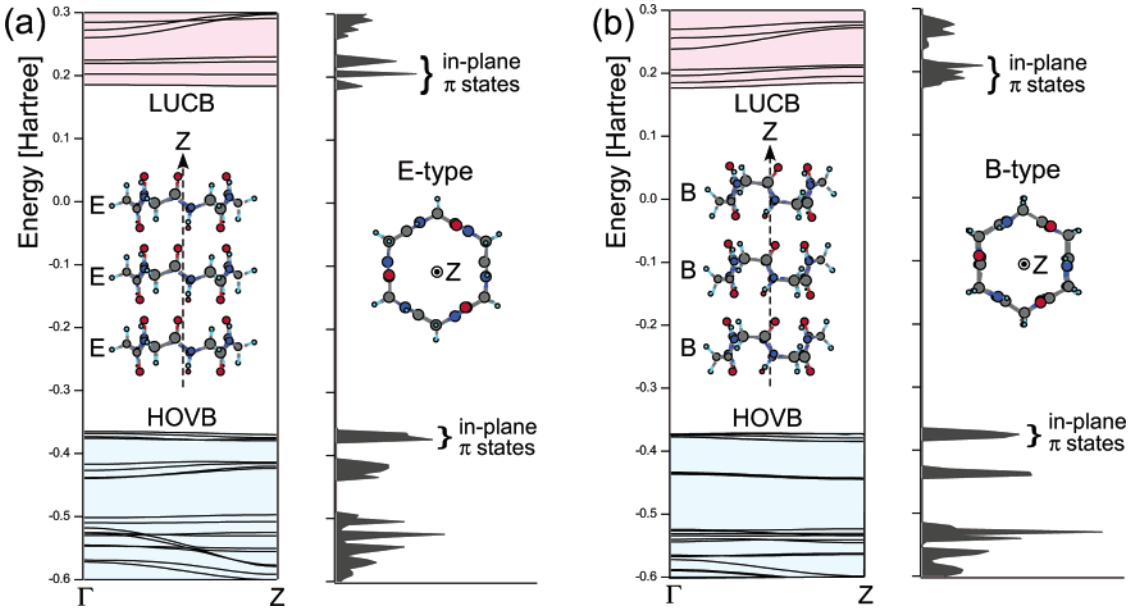

Figure 19. Calculated band structures and the density of states (DOS) of the E-type parallel PNT (a) and the B-type parallel PNT (b) (RHF/6-31G**).

between the adjacent PCRs (Figure 17b). Therefore, the inter-ring distance in the B-type antiparallel PNT is more elongated than that in the B-type parallel PNT. This feature does not appear in E-type PNTs, because the H···H distance in the E-type antiparallel PNT is increased by 5% compared with that in the B-type antiparallel PNT (Figure 16b).

We finally append that the individual PCR units in both E-type and B-type PNTs have the coincident ring (tube) axis while maintaining the S_6 symmetry. Therefore, the resulting PNTs have a straight rod shape irrespective of the stacking means of parallel and antiparallel. This straight rod shape is a common feature found in the DL-peptide nanotubes.[29]

B. Energetics. Let us discuss the energetics of these four PNTs. We first compare the condensation energies with respect to the different stacking means of parallel and antiparallel. In the E-type conformation (Figure 18), the parallel stacking and the antiparallel stacking provide almost the same condensation energies of 5.0 kcal/mol per residue; the resulting energy difference is at most 0.03 kcal/mol per residue. On the contrary, in the B-type conformation, the parallel stacking causes a larger condensation than that of the antiparallel stacking by 0.54 kcal/mol per residue (Figure 18). This is because the B-type antiparallel PNT includes the $C^{\alpha}-H\cdots H-C^{\alpha}$ repulsion between the adjacent PCRs as discussed in the former section (Figure 17b).

How does the energy difference occur between the E-type and B-type conformations? The present energetics (Figure 18) reveal that the stacking of the E-type PCRs causes a larger condensation than that of the B-type PCRs, irrespective of the stacking means of parallel and antiparallel. As a result, the energetic preferability of the isolated single B-type PCR (energetically more stable than an E-type PCR by 2.32 kcal/mol per residue) is compensated, and the total energies of E-type and B-type (parallel) PNTs become comparable.[31] This result indicates the existence of both backbone conformations of the E-type PNT having a larger diameter and the B-type PNT having a smaller diameter. To sum up the present results, we can also suggest that the B-type PNT backbone prefers the parallel stacking form, while the E-type PNT backbone has a chance to have both stacking forms of parallel and antiparallel.

C. Band Structures. Finally, we investigate the band structures of the PNTs. The calculations were carried out with the *Crystal98* program[32] based on the Hartree−Fock crystalline orbital (CO) method. The calculated band structures and the density of states (DOS) of the E-type and B-type parallel PNTs are shown in Figure 19, parts a and b. Several previous calculations based on the DFT approach have revealed a wide-gap semiconducting nature or an insulating electronic feature in some E-type PNTs.[9,10,33−36] The present Hartree−Fock CO calculations also show an equivalent electronic structure and similar characteristic band-edge states of the E-type PNT[37] (Figure 19a). Both the highest occupied valence band (HOVB) and the lowest unoccupied conduction band (LUCB) are formed by the in-plane π states analogous to the PCR backbone (Figure 13a).

The calculated effective masses of electrons and holes in the geometrically optimized PNTs are considerably large toward the tube axis. This less electronic delocalization is caused by

(28) The energy of the π electrons in the membered rings of $(CH)_m$ is given using the coulomb integral α and the resonance integral β by $E_j = \alpha + 2\beta \cos 2\pi j/m$, where $j = 0, 1, 2, ..., m/2$ if j is an even number, or $j = 0, 1, 2, ..., (m-1)/2$ if j is an odd number.

(29) Recently, we theoretically predicted bent penta-peptide nanotubes consisting of a homo-L-amino acid sequence. We also synthesized the penta-peptide nanotube (*cyclo*[-(L-Gln)$_5$]) and observed its bent tubular form by AFM.[30]

(30) Okamoto, H.; Nakanishi, T.; Nagai, Y.; Takeda, K.; Obataya, I.; Mihara, H.; Azehara, H.; Mizutani, W. *Jpn. J. Appl. Phys.* **2003**, *42*, 1.

(31) The resulting energy difference between E-type and B-type parallel PNTs is as small as 0.14 kcal/mol per residue (Figure 18).

(32) Saunders, V. R.; Dovesi, R.; Roetti, C.; Causà, M.; Harrison, N. M.; Orlando, R.; Zicovich-Wilson, C. M. *CRYSTAL 98*, University of Torino, 1998.

(33) Lewis, J. P.; Pawley, N. H.; Sankey, O. F. *J. Phys. Chem. B* **1997**, *101*, 10 576.

(34) Carloni, P.; Andreoni, W.; Parrinello, M. *Phys. Rev. Lett.* **1997**, *79*, 761.

(35) Jishi, R. A.; Braier, N. C.; White, C. T.; Mintmire, J. W. *Phys. Rev. B* **1998**, *58*, R16 009.

(36) Jishi, R. A.; Flores, R. M.; Valderrama, M.; Lou, L.; Bragin, J. *J. Phys. Chem. A* **1998**, *102*, 9858.

(37) The resulting HF energy gap of the E-type parallel PNT is 14.92 eV, which is considerably larger than our previous DFT result of 4.29 eV.[10] This is because ab initio Hartree−Fock calculations overestimate the energy gap due to the neglect of the inter-electron correlation, whereas the first-principles DFT calculations underestimate the corresponding value. Therefore, these values should be calibrated.

the in-plane π orbital nature of the band-edge states. For the delocalization of the band-edge states toward the tube axis, these in-plane π states should hybridize with the horn-like H 1*s* orbitals of the adjacent PCRs. However, the orthogonality between the in-plane π and H 1*s* states prohibits such orbital mixing in the optimized PNT geometry.

The in-plane π orbital nature of the HOVB and LUCB states is also conserved when the PNT is formed by the B-type PCRs. Therefore, a similar band structure is obtained in the B-type parallel PNT (Figure 19b). This feature is also irrespective of the stacking means, and furthermore, the twist of the adjacent PCRs hardly changes the frontier electronic states. Thus, electrons or holes are localized even in the twisted antiparallel PNTs.

VI. Conclusions

Possible molecular conformations in peptide nanorings and nanotubes were investigated by a mathematical conformation analysis as well as ab initio Hartree−Fock calculations, and the following points were clarified:

The mathematical analysis reveals that an even number of the alternating D- and L-amino acid sequences produces the peptide closed rings (PCRs) of $n \geq 6$. Moreover, even with the same n number, two types of the backbone conformation are theoretically predicted; i.e., the conventional extended-type (E-type) and the novel bound-type (B-type).

The energetically preferable backbone type changes in accordance with its ring size, i.e., the smaller rings ($n \leq 8$) prefer the B-type backbone, whereas the larger rings ($n \geq 10$) prefer the E-type backbone.

Ab initio calculations for the amino acid substitution reveal that all 20 encoded residues can form both E-type and B-type PCRs, whereas either type is provided as the global minimum form in accordance with the kind of the replaced side chains.

Electronically, the HOMO and LUMO states of the PCR backbones are formed by the in-plane π states. The replacement by the appropriate residues, furthermore, intrudes additional levels in the energy gap and forms the frontier orbitals localized at the side chains.

E-type and B-type PCRs can both stack to form the peptide nanotubes (PNTs). While the parallel stacking of the PCRs provides a monotonic stacking form, the antiparallel stacking causes a twisted PNT form.

The B-type PNT energetically prefers the parallel stacking form, while the E-type PNT has a chance to have both stacking means of parallel and antiparallel.

Acknowledgment. The authors would like to express their thanks to Prof. Kazuhisa Mihara (Tokyo Institute of Technology), Prof. Kenji Shiraishi (University of Tsukuba), Dr. Wataru Mizutani (AIST) and Dr. Katsuhiko Fukasaku for their stimulating discussion, and to Dr. Norihiko Takahashi (Waseda University) for his advice on using super computers. Parts of the present calculations have been performed at the Super Computer Center of the Institute for Molecular Science (IMS), Okazaki National Research Institutes.

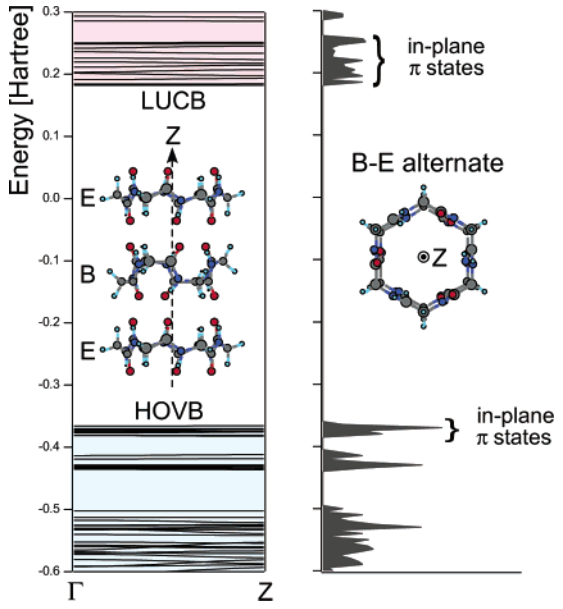

Figure 20. Calculated band structures and the density of states (DOS) of the B−E alternate PNT (RHF/6-31G**).

Appendix: Alternate Stacking of the B-type and E-type Nanorings

The resulting energy difference between the E-type and B-type PNTs is very small (Figure 18); therefore, we should also consider the alternate stacking of B-type and E-type PCRs. Those E-type and B-type PCRs have different internal diameters even with the same number of residues (n). Therefore, the difference might break the orbital orthogonality found between the in-plane π band-edge states and the horn-like H 1*s* states. In this additional section, we discuss this "B−E alternate" PNT (Figure 20).

The total energy calculation of the B−E alternate PNT gives a well-distinguished potential valley at the inter-ring distance of 5.20 Å, which is the value between the inter-ring distance of the E-type and the B-type PNTs. The present calculation also indicates that the B−E alternate PNT is less stable than the B-type parallel PNT but at most only by 1.80 kcal/mol per residue.

The resulting band structure and DOS reveal that both band-edge states still remain to be localized (Figure 20). Those band-edge states are formed by the in-plane π states, but those π states are swept away into the B-type PCR because of the supermolecular form due to the alternate stacking. Therefore, the orbital mixing via the inter-ring HBs hardly occurs even in this B−E alternate PNT. To induce a certain amount of the band-edge electronic delocalization, it would be necessary to produce some other designs, e.g., an inter-ring bridge via amino acid side chains.

JA0212720